

Generalized dynamical cluster theory for off-diagonal disorder

Jianxiong Zhai,^{1,2,3} Zihan Cheng^{1,4}, Yu Zhang,¹ and Youqi Ke^{1,2,3,*}

¹*School of Physical Science and Technology, ShanghaiTech University, Shanghai 201210, China*

²*Shanghai Institute of Optics and Fine Mechanics, Chinese Academy of Sciences, Shanghai 201800, China*

³*University of Chinese Academy of Sciences, Beijing 100049, China*

⁴*Department of Physics, University of Texas at Austin, Austin, Texas 78712, USA*



(Received 21 August 2023; accepted 6 February 2024; published 11 March 2024)

We present a generalized dynamical cluster theory for addressing the cluster effects of off-diagonal disorder. In this work, we introduce an extended local degree of freedom, namely the coupling space, to encapsulate the off-diagonal disorder in an auxiliary medium, and to form a cluster coupling space so that each site of the cluster can be homogeneously handled. Within the cluster coupling space, the self-consistent auxiliary dynamical cluster approximation (ADCA) with full symmetry of the lattice is developed to treat the diagonal and off-diagonal disorders on an equal footing. ADCA recovers the coherent-potential approximation at the single-site limit and the dynamical cluster approximation for diagonal-only disorder. Especially for the disordered vibrational system, ADCA conserves the force-constant sum rule. As important tests, we apply ADCA to the one- and three-dimensional disordered lattices, and we find that the ADCA density of state results with appropriate cluster size are in very good agreement with the exact and supercell calculations, especially for the localized defect modes. Moreover, the important interplay of mass and force-constant disorders is revealed by comparing the geometrically and arithmetically averaged density of states calculated by ADCA, presenting both effects of significantly enhanced localization and delocalization. The development of ADCA provides an effective approach for simulating both diagonal and off-diagonal disorders in materials.

DOI: [10.1103/PhysRevB.109.094203](https://doi.org/10.1103/PhysRevB.109.094203)

I. INTRODUCTION

Disordered systems, such as metallic alloys, are of significant interest in materials science and engineering due to their technological applications [1–16]. A reliable and effective theoretical method for treating disorder is thus critical for understanding the important effects of disorders, and is desirable for the design of disordered materials. However, theoretical tools for describing disordered systems are faced with extreme difficulties, because the breakdown of translational symmetry requires the calculation of configurational-averaged physical properties. Over the past 50 years, significant progress for mean-field-type approaches has been made in the study of disordered systems. The fundamental idea behind the coherent-potential approximation (CPA), as a dynamical mean-field theory dating back to 1960s [17–21], is to map the original infinite disordered lattice onto a single impurity embedded in an effective medium, which is chosen such that, on average, it does not scatter. This method has many desirable properties, including computational simplicity, the ability to interpolate between important physical limits, and the preservation of full point-group symmetry of the underlying lattice. CPA has proven to be a useful tool for understanding the properties of disordered systems, and it has contributed to the development of new materials [22–24]. However, in a single-site approximation, CPA fails to account for the nonlocal correlation of the local fluctuations. Moreover, the embedding

model utilized in CPA requires that the impurity atom couple to the effective medium in a constant way, excluding the randomness in the off-diagonal term of the Hamiltonian, while the off-diagonal disorder can be expected to play a significant role in determining the properties of many disordered alloys [1]. These limitations strongly motivate the search for advanced mean-field approaches that can treat both cluster effects and off-diagonal disorder.

Great efforts have been made to overcome these limitations. These include the cluster extensions to CPA, such as molecular CPA (MCPA) [25–29] and the dynamical cluster approximation (DCA) [30–35], which are also grounded in the embedding model. However, all these methods have only considered diagonal disorder and are unable to capture the disorder fluctuations on the coupling terms between the impurity cluster and the effective medium. To address this limitation, Blackman, Esterling, and Berk (BEB) introduced an augmented space technique to transform the problem of decoupled diagonal and off-diagonal disorder into a diagonal disorder to apply CPA [36]. This technique has also been extended to the cluster level by applying DCA, which proves suitable for electronic systems [34,35]. Unfortunately, for disordered vibrational systems [37], the diagonal and off-diagonal elements of the dynamic matrix are correlated by the momentum conservation law, which requires that the force-constant sum rule $D_{ii} = -\sum_{j \neq i} D_{ij}$ be satisfied. This kind of coupled diagonal and off-diagonal disorder makes the BEB method infeasible. Moreover, BEB transformation is not suitable for handling Anderson-type off-diagonal disorder (with continuous distribution), which generally exists in

*keyq@shanghaitech.edu.cn

realistic alloys. Another way to address the force-constant sum rule is the itinerant coherent-potential approximation (ICPA) [38,39]. However, ICPA leads to changes in the self-energy terms associated with nearest neighbors. This issue can result in additional errors when calculating bulk and transport properties for specific parameters using ICPA [40]. Furthermore, the computational cost increases significantly with the number of atomic species or when dealing with systems with distributed force constants.

Recently, some of the authors have presented the auxiliary coherent potential approximation (ACPA) within the embedding model [40–43], which retains all the desirable properties of CPA and can handle force constant disorder with the sum rule strictly conserved. In previous work, ACPA has shown good agreement with supercell calculation and experimental measurements in the phonon dispersions of different alloys [42]. Moreover, ACPA is proficient in directly dealing with Anderson-type off-diagonal disorder, and it presents significant improvement for the spectral linewidth function to agree well with the supercell method and experiment [43]. Furthermore, implementing ACPA for electronic systems is straightforward, offering potential integration with dynamical mean-field theory (DMFT) for treating the strongly correlated Anderson-Hubbard model with off-diagonal disorders [44]. This single-site ACPA method has shown important potential as a starting point for constructing a general effective-medium theory. However, the problem of how to construct a translationally invariant cluster extension formalism for ACPA remains unresolved. In this work, by introducing the cluster-coupling space, we develop an auxiliary dynamical cluster approximation (ADCA) formalism to handle the important cluster effects of off-diagonal disorder. This ADCA formalism reduces to ACPA at the single-site limit and recovers DCA when only mass disorder is present. We demonstrate the effectiveness of ADCA by calculating the phonon density of states in one- and three-dimensional (1D and 3D) disordered systems, and we compare with the exact and supercell results.

The rest of the paper is organized as follows: Section II provides a quick review of the basic formalism of the ACPA method. Section III presents the concept of cluster coupling space. Section IV provides a detailed description of the self-consistent ADCA formalism, and the ADCA self-energy is analyzed in Sec. V. In Sec. VI, the results and discussions of the study are presented. Finally, we conclude our work in Sec. VII and provide more information in Appendixes A and B.

II. AUXILIARY MEDIUM THEORY FOR DISORDERED VIBRATION

The Green's function for lattice vibration in the harmonic approximation is given by

$$G = (m\omega^2 - D)^{-1}, \quad (1)$$

where D is the force-constant matrix. Due to the translational symmetry, the force matrix is subjected to the sum rule $\sum_j D_{ij} = 0$. In a random alloy, this sum rule leads to the inseparability of diagonal and off-diagonal disorders, which makes the theory of disordered phonon excitations difficult.

To address this issue, the ACPA approach brings forth a general decomposition technique that transforms the intricate off-diagonal disorder into a tractable diagonal-like disorder problem. This unique strategy offers a unified approach that encapsulates a broad range of physical parameters and scenarios for handling the general off-diagonal disorders, including force-constant disorder (FCD) in lattice vibration [40–43]. This is achieved by writing the random force constant k in a separable form, namely

$$k_{R_I\alpha R_J\beta}^{Q_I Q_J} = x_{R_I}^{Q_I} S_{R_I\alpha R_J\beta} x_{R_J}^{Q_J} + \lambda_{R_I\alpha R_J\beta} \quad (I \neq J), \quad (2)$$

where $x_{R_I}^{Q_I}/x_{R_J}^{Q_J}$ is dependent on the atomic occupant Q_I/Q_J on the site R_I/R_J , and α/β are bases of each site. The quantities $S_{R_I\alpha R_J\beta}$ and $\lambda_{R_I\alpha R_J\beta}$ are independent of the atomic occupations on sites R_I and R_J . As demonstrated, Eq. (2) can accurately describe the disorder in the force constant of realistic 3D alloys, presenting very good agreement with ICPA and experimental measurements in calculating the phonon dispersions [42] and linewidth function [40] of different fcc alloys. This representation of FCD allows the force constant to be written as a product of two matrices,

$$D = \mathcal{X}\mathcal{K}. \quad (3)$$

\mathcal{X} is a diagonal matrix with elements $\mathcal{X}_{R_I R_J} = x_{R_I}^{Q_I} \delta_{IJ}$, and the \mathcal{K} matrix is defined as

$$\mathcal{K}_{R_I\alpha R_J\beta} = - \left(S_{R_I\alpha R_J\beta} x_{R_J}^{Q_J} + \frac{\lambda_{R_I\alpha R_J\beta}}{x_{R_I}^{Q_I}} \right) \quad (I \neq J), \quad (4)$$

$$\mathcal{K}_{R_I\alpha R_I\beta} = \sum_{J \neq I} \left(S_{R_I\alpha R_J\beta} x_{R_J}^{Q_J} + \frac{\lambda_{R_I\alpha R_J\beta}}{x_{R_I}^{Q_I}} \right). \quad (5)$$

It can be shown that the matrix \mathcal{K} satisfies the force constant sum rule. The key point of this decomposition is that the terms containing x_{R_I} are linearly separated in \mathcal{K} and thus we can write \mathcal{K} as a sum of single-site dependent quantities as

$$\mathcal{K} = \sum_I \tilde{\mathcal{K}}^{R_I}, \quad (6)$$

where $\tilde{\mathcal{K}}^{R_I}$ contains all the contributions that are associated only with x_{R_I} . For a site R_I with M_N neighboring sites of nonzero coupling, $\tilde{\mathcal{K}}^{R_I}$ is then a $d(M_N + 1) \times (M_N + 1)d$ quantity with (where d is the dimension or the bases of a single site)

$$\begin{aligned} \tilde{\mathcal{K}}_{R_I\alpha R_J\beta}^{R_I} &= S_{R_I\alpha R_J\beta} x_{R_I}^{Q_I} \quad (J \neq I), \\ \tilde{\mathcal{K}}_{R_I\alpha R_I\beta}^{R_I} &= -S_{R_I\alpha R_J\beta} x_{R_I}^{Q_I} \quad (J \neq I), \\ \tilde{\mathcal{K}}_{R_I\alpha R_I\beta}^{R_I} &= -\frac{\lambda_{R_I\alpha R_J\beta}}{x_{R_I}^{Q_I}} \quad (J \neq I), \\ \tilde{\mathcal{K}}_{R_I\alpha R_I\beta}^{R_I} &= \sum_J \frac{\lambda_{R_I\alpha R_J\beta}}{x_{R_I}^{Q_I}}, \\ \tilde{\mathcal{K}}_{R_I\alpha R_{J'}\beta}^{R_I} &= 0 \quad (J, J' \neq I). \end{aligned} \quad (7)$$

As a consequence, the Green's function can be rewritten as

$$G = g\mathcal{X}^{-1}, \quad (8)$$

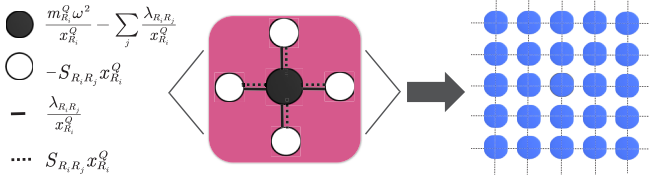


FIG. 1. Schematic illustration of ACPA in a 2D lattice model. The single impurity P^{R_l} contains the couplings to nearest-neighbor sites; the field in pink represents the Weiss mean field in which the single-site P^{R_l} is embedded.

where g is the auxiliary Green's function defined as

$$g = (\mathcal{X}^{-1}m\omega^2 - \mathcal{K})^{-1} = P^{-1}, \quad (9)$$

with the auxiliary Hamiltonian

$$P = \sum_I P^{R_l}, \quad (10)$$

where $P^{R_l} = x_{R_l}^{Q_l, -1} m_{R_l}^{Q_l} \omega^2 - \tilde{\mathcal{K}}^{R_l}$, and the dimension of P^{R_l} is the same as that of $\tilde{\mathcal{K}}^{R_l}$. In this form, the general disorder (including both mass disorder and FCD) in lattice vibration is reduced to an auxiliary diagonal-like disorder problem. Thus, the self-consistent ACPA loop for solving the coherent medium $\mathcal{P} = \sum_I \mathcal{P}^{R_l}$ can be carried out by mapping the original infinite disordered lattice onto an averaged single impurity embedded in an effective medium [40], as schematically shown in Fig. 1.

Nevertheless, the single-site nature of ACPA poses a limitation as it neglects nonlocal correlations of disorder scattering and precludes the treatment of short-range order of disorder [45,46]. For a general cluster theory, it becomes indispensable to construct an auxiliary cluster scatter, denoted as P^c , which is determined by the atomic configuration of the cluster, to account for the cluster effects of off-diagonal disorders. One direct approach involves implementing MACPA [41], wherein auxiliary scatters are summed to yield $P^c = \sum_{l=1}^{N_c} P^{R_l}$, and then embed this cluster in the effective medium. However, this method violates the translational invariance of the primitive lattice as only boundary cluster sites couple with the effective medium, thus imposing an open boundary condition on the cluster [47].

In this work, we aim to develop a cluster mean-field approach that retains translational invariance for a system with off-diagonal disorder. Notably, for systems with only diagonal disorder, the DCA method, which enforces Born-von Karman (BVK) periodic boundary conditions on the cluster, provides a state-of-the-art solution to restore the full symmetry of the lattice. DCA modifies the coupling term to ensure that each site couples to the surroundings in exactly the same manner, presenting a homogenous treatment of the cluster [see the difference between MCPA and DCA as shown in Eqs. (A9) and (A3) in Appendix A]. However, DCA is still based on the embedding model that precludes the fluctuation in off-diagonal terms, and thus directly integrating the auxiliary medium theory within the DCA framework is challenging and requires significant development because the off-diagonal elements in the quantity P in Eq. (10) contain randomness. In the next section, we will introduce the idea of cluster coupling

space (CCS), which combines the attributes of both the ACPA and DCA methods, to form a general cluster paradigm for treating off-diagonal disorder.

III. CLUSTER COUPLING SPACE

A. Coupling space

It is clear that the single-site auxiliary quantity P^{R_l} and $\tilde{\mathcal{K}}^{R_l}$ for R_l contains the extended dimensions $d \times (M_N + 1)$, beyond the single-site degree of freedom d (here we denote the single-site basis space with \mathcal{S}). To name such extended dimensions, we introduce the coupling space $\overline{\mathcal{T}}$ associated with each lattice site for defining the auxiliary single-site matrix quantities in ACPA. The space $\overline{\mathcal{T}}$ encapsulates the influences exerted by a specific occupation of a site upon its surrounding coupled sites. In the primitive lattice, a site \mathbf{R}_l is connecting to M_N neighboring sites with nonzero coupling (or force constant). The neighboring site \mathbf{R}_J is related to \mathbf{R}_l via the translational vector $\overline{\mathbf{T}}_J$ (where J ranges from $-M_N/2$ to $M_N/2$ with $\overline{\mathbf{T}}_0 = 0$), namely $\mathbf{R}_J = \mathbf{R}_l + \overline{\mathbf{T}}_J$. The basis state in $\overline{\mathcal{T}}$ can be represented by the orthonormal bases $|\overline{\mathbf{T}}_J\rangle$. The bases $|\overline{\mathbf{T}}_J\rangle$ encompass the coupling information of a single site \mathbf{R}_l along the $\overline{\mathbf{T}}_J$ direction. In this context, we can rewrite the auxiliary single-site $\tilde{\mathcal{K}}^{R_l}$ in Eq. (7) in the coupling space $\Gamma = \overline{\mathcal{T}} \otimes \mathcal{S}$, with $d(M_N + 1)$ degrees of freedom, as follows:

$$\begin{aligned} \tilde{\mathcal{K}}^{\Gamma, R_l} = & \sum_{J \neq 0} S_{\mathbf{R}_l, \mathbf{R}_J} x_{\mathbf{R}_J} |\overline{\mathbf{T}}_J\rangle \langle \overline{\mathbf{T}}_J| - \sum_{J \neq 0} S_{\mathbf{R}_l, \mathbf{R}_J} x_{\mathbf{R}_J} |\overline{\mathbf{T}}_J\rangle \langle \overline{\mathbf{T}}_0| \\ & - \sum_{J \neq 0} \frac{\lambda_{\mathbf{R}_l, \mathbf{R}_J}}{x_{\mathbf{R}_J}} |\overline{\mathbf{T}}_0\rangle \langle \overline{\mathbf{T}}_J| + \sum_J \frac{\lambda_{\mathbf{R}_l, \mathbf{R}_J}}{x_{\mathbf{R}_J}} |\overline{\mathbf{T}}_0\rangle \langle \overline{\mathbf{T}}_0|, \quad (11) \end{aligned}$$

where $\mathbf{R}_J = \mathbf{R}_l + \overline{\mathbf{T}}_J$, and the sub/superscripts Q_l and α are omitted for simplicity as compared to Eq. (7). Moreover, it should also be noted that the primitive lattice Fourier transformation (LFT) is related to the basis vector $\overline{\mathbf{T}}_J$ of the coupling space $\overline{\mathcal{T}}$.

B. Cluster coupling space

We consider a cluster comprising N_c lattice sites labeled as $\{\mathbf{R}_n, 1 \leq n \leq N_c\}$ [as shown in Fig. 2(a) for $N_c = 4$ in a 1D chain], with the corresponding cluster translational vector denoted by T^{cl} , and the associated BZ k -point denoted by $\tilde{\mathbf{k}}$. Then, the space, denoted by \mathcal{R} , can be introduced to represent the N_c sites, and the cluster space can be defined as $\mathcal{C} = \mathcal{R} \otimes \mathcal{S}$, in which the physics properties can be calculated. To develop a translational invariant cluster mean-field approach, the Born-von Karman (BVK) periodic boundary condition is imposed on the cluster lattice, as a critical assumption. Within DCA, the site-diagonal disorders are handled homogeneously for all the sites of the cluster. To realize a homogeneous treatment of the disordered P^{R_l} with extended dimensions (spanned by the coupling space $\overline{\mathcal{T}}$) for each site of the cluster, we introduce the cluster coupling space (CCS) Θ , which is the direct product of the periodic cluster space with the coupling space, namely

$$\Theta = \mathcal{R} \otimes \overline{\mathcal{T}} \otimes \mathcal{S}, \quad (12)$$

which contains $N_c \times (M_N + 1) \times d$ degrees of freedom. It is noted that the summation or integration of coupling degree of

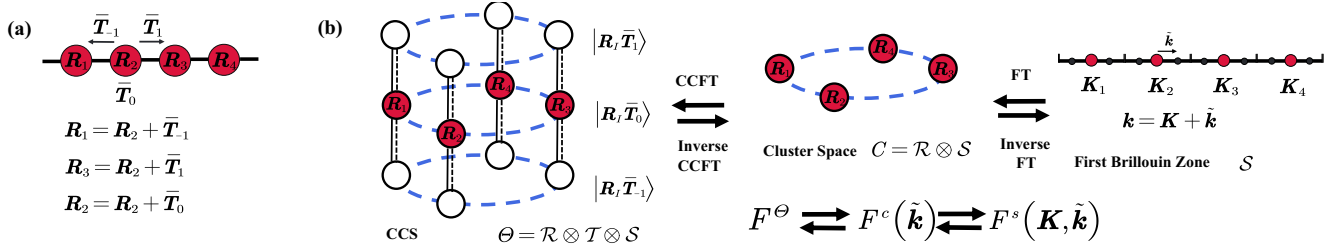


FIG. 2. (a) A cluster of $N_c = 4$ in a 1D chain; (b) the relation between the cluster coupling space (CCS) Θ , cluster space \mathcal{C} , and primitive-cell space \mathcal{S} . The BVK periodic boundary condition is applied to the cluster. Here, Θ is connected to \mathcal{C} by the cluster-coupling-space Fourier transformation (CCFT) and its inverse transformation for each $\tilde{\mathbf{k}}$; \mathcal{C} and \mathcal{S} are connected by the normal Fourier transformation (FT) for each \mathbf{K}_n .

freedom $\bar{\mathcal{T}}$ reduce the CCS to the cluster space \mathcal{C} (as shown in the following Fourier transformation). Every basis in CCS can be represented as $|\mathbf{R}_I \bar{\mathcal{T}}_J \alpha\rangle$.

In the CCS, as depicted in Fig. 2(b), a ring is formed by four cluster sites with periodic boundary conditions. In the CCS, the auxiliary quantities, namely P^Θ and \mathcal{K}^Θ , of different sites are disconnected, becoming site-diagonal. As a result, the auxiliary quantity of the cluster in CCS, denoted as $\tilde{\mathcal{K}}^\Theta$, can be expressed as

$$\tilde{\mathcal{K}}_{\bar{\mathcal{T}}_I \bar{\mathcal{T}}_J}^{\Theta, \mathbf{R}_M \mathbf{R}_N} = \tilde{\mathcal{K}}_{\bar{\mathcal{T}}_I \bar{\mathcal{T}}_J}^{\Gamma, \mathbf{R}_M} \delta_{\mathbf{R}_M, \mathbf{R}_N}, \quad (13)$$

where $\tilde{\mathcal{K}}_{\bar{\mathcal{T}}_I \bar{\mathcal{T}}_J}^{\Theta, \mathbf{R}_M \mathbf{R}_N} = \langle \mathbf{R}_M \bar{\mathcal{T}}_I | \tilde{\mathcal{K}}^\Theta | \mathbf{R}_N \bar{\mathcal{T}}_J \rangle$, and $\tilde{\mathcal{K}}_{\bar{\mathcal{T}}_I \bar{\mathcal{T}}_J}^{\Gamma, \mathbf{R}_M}$ is the single-site auxiliary quantity in Γ as defined in Eq. (11). Here, $\tilde{\mathcal{K}}^\Theta$ is dependent on the atomic configuration of the cluster. Then the auxiliary cluster scatter can be obtained as $P^\Theta = [x^{-1}m]^\Theta \omega^2 - \tilde{\mathcal{K}}^\Theta$, where $[x^{-1}m]_{\bar{\mathcal{T}}_I \bar{\mathcal{T}}_J}^{\Theta, \mathbf{R}_M \mathbf{R}_N} = x_{\mathbf{R}_N}^{\mathcal{Q}_N, -1} m_{\mathbf{R}_N}^{\mathcal{Q}_N} \delta_{\mathbf{R}_M, \mathbf{R}_N} \delta_{\bar{\mathcal{T}}_I, \bar{\mathcal{T}}_J}$ is site-diagonal. The CCS provides a framework to treat each site equivalently to construct a translational invariant auxiliary cluster mean-field theory for addressing the off-diagonal disorder.

To proceed, it is important to define the mutual transformation of the quantities between the CCS and the cluster space \mathcal{C} . To establish a relation between quantities in CCS Θ and cluster space \mathcal{C} , it is important to note that for a cluster with the BVK periodic boundary condition, each site \mathbf{R}_I in the cluster can be translated to its neighboring site \mathbf{R}_J by the vector $\bar{\mathcal{T}}_J$ in $\bar{\mathcal{T}}$. For example, as shown in Fig. 2(a) for a 1D cluster of N_c , \mathbf{R}_2 is related to its neighboring sites as $\mathbf{R}_1 = \mathbf{R}_2 + \bar{\mathcal{T}}_{-1}$ and $\mathbf{R}_3 = \mathbf{R}_2 + \bar{\mathcal{T}}_1$, providing a correspondence for mapping the coupling vector $\bar{\mathcal{T}}_J$ in $\bar{\mathcal{T}}$ to the lattice site \mathbf{R} . Thus, we can introduce the relation that connects the periodic quantity F^Θ in CCS and F^c in \mathcal{C} , namely by the coupling space Fourier transformation (CCFT) and the inverse CCFT for the cluster (for each $\tilde{\mathbf{k}}$ in the cluster BZ),

$$F_{\mathbf{R}_I \mathbf{R}_J}^c(\tilde{\mathbf{k}}) = \sum_{\bar{\mathcal{T}}_M, \bar{\mathcal{T}}_N} e^{-i\tilde{\mathbf{k}}(\bar{\mathcal{T}}_M - \bar{\mathcal{T}}_N)} F_{\bar{\mathcal{T}}_M \bar{\mathcal{T}}_N}^{\Theta, \mathcal{R}_{IM}, \mathcal{R}_{JN}} \quad (14)$$

and

$$F_{\bar{\mathcal{T}}_M \bar{\mathcal{T}}_N}^{\Theta, \mathcal{R}_{IM}, \mathcal{R}_{JN}} = \frac{N_c}{N} \sum_{\tilde{\mathbf{k}}} e^{i\tilde{\mathbf{k}}(\bar{\mathcal{T}}_M - \bar{\mathcal{T}}_N)} F_{\mathbf{R}_I \mathbf{R}_J}^c(\tilde{\mathbf{k}}), \quad (15)$$

where $\mathcal{R}_{IM} = \mathbf{R}_I + \bar{\mathcal{T}}_M$ and $\mathcal{R}_{JN} = \mathbf{R}_J + \bar{\mathcal{T}}_N$. As seen from above Eqs. (14) and (15), for example in the phase factor $e^{-i\tilde{\mathbf{k}}(\bar{\mathcal{T}}_M - \bar{\mathcal{T}}_N)}$, each site \mathbf{R} and coupling vector $\bar{\mathcal{T}}$ are treated

without any bias to present a homogeneous medium of cluster in both Θ and \mathcal{C} . We note that, in contrast to the case of MCPA in Eq. (A3), DCA homogeneously introduces a phase factor to the coupling (hopping) element $W_{\mathbf{R}_I, \mathbf{R}_J}$ between a cluster site \mathbf{R}_I and $\mathbf{R}_J = \mathbf{R}_I + \bar{\mathcal{T}}_J$, namely $W_{\mathbf{R}_I, \mathbf{R}_J} e^{-i\tilde{\mathbf{k}}\bar{\mathcal{T}}_J}$ in Eq. (A9), to ensure the full translational symmetry of the lattice. As we show in Eqs. (A10), (A11), and (A12) in Appendix A, our approach generalizes the concept for introducing this phase factor in DCA as a Fourier transform within the extended CCS. This generalization facilitates the analysis of the cluster-to-effective medium coupling via the Fourier transformation relationship between the CCS Θ and cluster space \mathcal{C} (as shown in Fig. 2 for the relation between different spaces).

IV. AUXILIARY DYNAMICAL CLUSTER APPROXIMATION

With the CCS, we can establish the self-consistent auxiliary dynamical cluster approximation (ADCA) with the full lattice symmetry to account for the cluster effects of off-diagonal disorders. As one of the main tenets of ADCA, the substitution of an effective cluster medium by a specific atomic configuration, on average, leads to the ADCA effective medium, and this ADCA condition can be expressed in the CCS as follows:

$$\bar{g}^\Theta = \sum_{\mathcal{Q}} c^{\mathcal{Q}} g^{\Theta, \mathcal{Q}}, \quad (16)$$

where \mathcal{Q} denotes a specific atomic configuration of the cluster, and $C^{\mathcal{Q}}$ is the probability of \mathcal{Q} configuration. To obtain the averaged cluster Green's function, the coherent interactor in CCS, namely Ω^Θ , is introduced to account for the influence of the surrounding effective medium on the cluster. With the interactor Ω^Θ , we can write the average GFs in CCS by mapping the disordered lattice problem to an embedded cluster model,

$$\bar{g}^\Theta = [\mathcal{P}^\Theta - \Omega^\Theta]^{-1}, \quad (17)$$

where \mathcal{P}^Θ is the effective Hamiltonian describing the averaged auxiliary medium, and for a specific \mathcal{Q} ,

$$g^{\Theta, \mathcal{Q}} = [\mathcal{P}^{\Theta, \mathcal{Q}} - \Omega^{\Theta, \mathcal{Q}}]^{-1}, \quad (18)$$

where the auxiliary Hamiltonian $\mathcal{P}^{\Theta, \mathcal{Q}} = [x^{-1}m]^\Theta \omega^2 - \tilde{\mathcal{K}}^{\Theta, \mathcal{Q}}$. Subsequently, we can obtain the effective medium in

CCS by utilizing the above Eqs. (16)–(18), namely

$$\mathcal{P}^\theta = \left[\sum_{\mathcal{Q}} c^{\mathcal{Q}} [P^{\theta, \mathcal{Q}} - \Omega^\theta]^{-1} \right]^{-1} + \Omega^\theta. \quad (19)$$

With a given CCS interactor Ω^θ , the cluster impurity solver, namely Eq. (19), conducts the calculation for all sampled atomic configurations to obtain the quantity \mathcal{P}^θ . It is clear that, as long as Ω^θ is homogeneously generated for the cluster, the equivalent treatment of cluster sites in CCS ensures the translational invariance of \mathcal{P}^θ in ADCA.

After obtaining \mathcal{P}^θ , we can construct the \mathcal{P}^c in the cluster space \mathcal{C} to calculate the averaged Green's functions of the cluster by applying CCFT in Eq. (14) as follows:

$$\mathcal{P}_{\mathbf{R}_I, \mathbf{R}_J}^c(\tilde{\mathbf{k}}) = \sum_{\bar{\mathbf{T}}_M, \bar{\mathbf{T}}_N} e^{-i\tilde{\mathbf{k}}(\bar{\mathbf{T}}_M - \bar{\mathbf{T}}_N)} \mathcal{P}_{\bar{\mathbf{T}}_M \bar{\mathbf{T}}_N}^{\theta, \mathcal{R}_{IM}, \mathcal{R}_{JN}}, \quad (20)$$

and due to the BVK periodic boundary condition, the periodic cluster $\mathcal{P}_{\mathbf{R}_I, \mathbf{R}_J}^c(\tilde{\mathbf{k}})$ can be Fourier-transformed into a primitive-cell quantity on a set of discrete $\{\mathbf{K}_n, 1 \leq n \leq N_c\}$ by [as shown in Fig. 2(d)]

$$\mathcal{P}^S(\mathbf{K}_n, \tilde{\mathbf{k}}) = \sum_{\mathbf{R}_J} e^{-i\mathbf{K}_n(\mathbf{R}_I - \mathbf{R}_J)} \mathcal{P}_{\mathbf{R}_I, \mathbf{R}_J}^c(\tilde{\mathbf{k}}), \quad (21)$$

where $\mathcal{P}^S(\mathbf{K}_n, \tilde{\mathbf{k}})$ features the degree of freedom of single-site space \mathcal{S} . It should be noted that $\mathbf{k} = \mathbf{K}_n + \tilde{\mathbf{k}}$ for the k point in the BZ of the primitive cell of lattice. As a result, the averaged auxiliary GF for each \mathbf{k} is given by

$$\bar{g}^S(\mathbf{k}) = \mathcal{P}^{S, -1}(\mathbf{K}_n, \tilde{\mathbf{k}}). \quad (22)$$

Here, $\bar{g}^S(\mathbf{k})$ and $\mathcal{P}^S(\mathbf{K}_n, \tilde{\mathbf{k}})$ feature the full symmetry of the lattice.

To form a closed set of self-consistent equations for ADCA, we need to update the CCS interactor Ω^θ . To do so, we perform the inverse FT to obtain the cluster GF $\bar{g}^c(\tilde{\mathbf{k}})$ from $\bar{g}^S(\mathbf{K}_n, \tilde{\mathbf{k}})$, namely

$$\bar{g}_{\mathbf{R}_I, \mathbf{R}_J}^c(\tilde{\mathbf{k}}) = \frac{1}{N_c} \sum_{\mathbf{K}_n} e^{i\mathbf{K}_n(\mathbf{R}_I - \mathbf{R}_J)} \bar{g}^S(\mathbf{K}_n, \tilde{\mathbf{k}}), \quad (23)$$

so that we can derive the GF in CCS by the inverse CCFT in Eq. (15),

$$\bar{g}_{\bar{\mathbf{T}}_M \bar{\mathbf{T}}_N}^{\theta, \mathcal{R}_{IM}, \mathcal{R}_{JN}} = \frac{N_c}{N} \sum_{\tilde{\mathbf{k}}} e^{i\tilde{\mathbf{k}}(\bar{\mathbf{T}}_M - \bar{\mathbf{T}}_N)} \bar{g}_{\mathbf{R}_I, \mathbf{R}_J}^c(\tilde{\mathbf{k}}). \quad (24)$$

Then, by applying Eq. (17), Ω^θ is obtained as

$$\Omega_{\text{new}}^\theta = \mathcal{P}^\theta - \bar{g}^{\theta, -1}. \quad (25)$$

Equations (19)–(25) form a closed set of ADCA self-consistent equations to solve for the averaged GF, namely $\bar{g}^S(\mathbf{k})$. The iterative calculation starts with an initial guess for Ω^θ , for which we adopt $\Omega^\theta = 0$ in our present implementation. Then, Ω^θ is self-consistently updated until the convergence is reached, as shown in Fig. 3 for the ADCA loop. It should be mentioned that the ADCA formalism recovers two limiting cases, namely the ACPA for a single-site approximation [41], and DCA for diagonal-only disorder [32], providing an important test for the whole formulation of

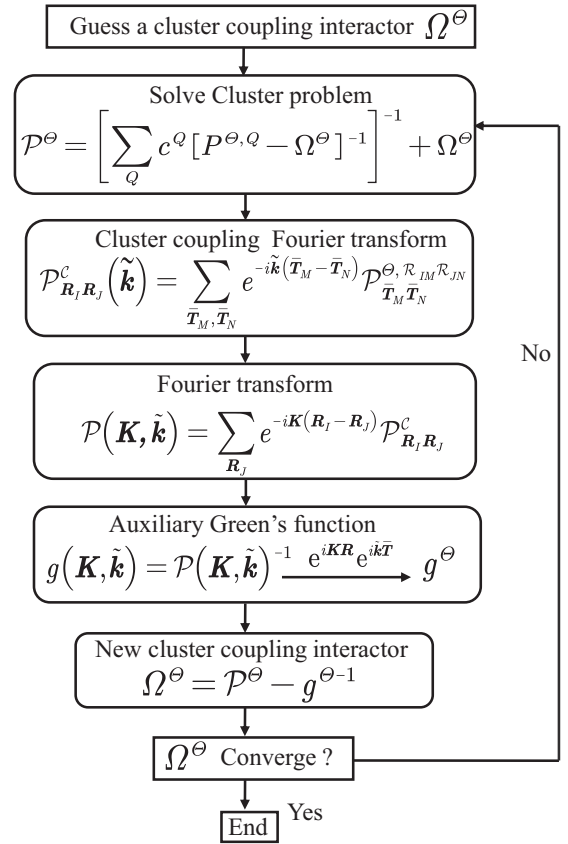


FIG. 3. Sketch of the self-consistent loop for the ADCA embedded cluster approach.

ADCA with the CCS. For example, for $N_c = 1$, it is unequivocal that the ADCA restores the ACPA with the sole $\mathbf{K}_1 = \mathbf{0}$. On the other hand, for the mass-only disorder (diagonal disorder), the ADCA formulation recovers into the DCA formalism, as shown in Appendix B.

V. SELF-ENERGY IN ADCA

It is known that the single-site ACPA assumes that the self-energy is the sum of single-site self-energies, namely $\Sigma^{\text{ACPA}} = \sum_{R_I} \Sigma^{R_I}$, ignoring all the nonlocal correlations described by crossing diagrams [40]. The development of ADCA systematically restores the nonlocal corrections by embedding the cluster with finite size N_c in CCS. In this section, we investigate the ADCA self-energy of disorder scattering. To begin, by using the ADCA condition of Eq. (16) and the relations of Eqs. (17) and (18), we can rewrite the CCS conditional GF $g^{\theta, \mathcal{Q}}$ for a specific atomic configuration \mathcal{Q} in the Dyson equation

$$g^{\theta, \mathcal{Q}} = \mathcal{G}^\theta + \mathcal{G}^\theta V^{\theta, \mathcal{Q}} g^{\theta, \mathcal{Q}}, \quad (26)$$

and the averaged CCS GF \bar{g}^θ ,

$$\bar{g}^\theta = \mathcal{G}^\theta + \mathcal{G}^\theta \Sigma^\theta \bar{g}^\theta, \quad (27)$$

where $V^{\theta, \mathcal{Q}} = P^{\theta, 0} - P^{\theta, \mathcal{Q}}$ ($P^{\theta, 0}$ describes a perfect cluster), the cavity Green's function \mathcal{G}^θ is related to the interactor

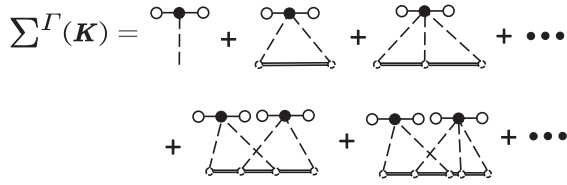


FIG. 4. Irreducible diagrams for the ADCA self-energy. Double line denotes the averaged auxiliary Green's function \bar{g}^Γ . The symbol containing a filled circle connecting two empty circles denotes the auxiliary single-site scatter with off-diagonal randomness in the coupling space.

through $\mathcal{G}^\theta = (p^{\theta,0} - \Omega^\theta)^{-1}$, and Σ^θ is the ADCA self-energy in CCS. Then, one can obtain the relation

$$\overline{(\bar{g}^{\theta-1} + \Sigma^\theta - V^{\theta,0})^{-1}} = \bar{g}^\theta, \quad (28)$$

where the overline denotes the configurational average. Then the ADCA self-energy equation can be expanded as

$$\overline{V^\theta - \Sigma^\theta} + \overline{(V^\theta - \Sigma^\theta)\bar{g}^\theta(V^\theta - \Sigma^\theta)} + \dots = 0. \quad (29)$$

By rearranging the equation and defining the quantity $\sigma^\theta = \overline{V^\theta} + \overline{V^\theta \bar{g}^\theta V^\theta} - \Sigma^\theta \bar{g}^\theta V^\theta - \overline{V^\theta \bar{g}^\theta \Sigma^\theta} + \dots$, we can get

$$\Sigma^\theta - \Sigma^\theta \bar{g}^\theta \Sigma^\theta + \Sigma^\theta \bar{g}^\theta \Sigma^\theta \bar{g}^\theta \Sigma^\theta + \dots = \sigma^\theta, \quad (30)$$

which can also be rewritten as $\Sigma^\theta [1 + \bar{g}^\theta \Sigma^\theta]^{-1} = \sigma^\theta$. Here, by using the relation $[1 + \bar{g}^\theta \Sigma^\theta]^{-1} = 1 - \bar{g}^\theta \Sigma^\theta [1 + \bar{g}^\theta \Sigma^\theta]^{-1} = 1 - \bar{g}^\theta \sigma^\theta$, we can find a self-consistent relation for Σ^θ , namely

$$\Sigma^\theta = \sigma^\theta [1 - \bar{g}^\theta \sigma^\theta]^{-1}. \quad (31)$$

Therefore, one can make the following expansion:

$$\Sigma^\theta = \overline{V^\theta} + \overline{V^\theta \bar{g}^\theta V^\theta} + \overline{V^\theta \bar{g}^\theta V^\theta \bar{g}^\theta V^\theta} + \dots \quad (32)$$

(note that the corrections for multiple occupancy are omitted for simplicity) [19]. It is clear the ACPA self-energy diagram is included within the above expression. To obtain the ADCA self-energy in reciprocal space, we define the cluster Fourier transformation on CC space as

$$F_{\bar{\mathbf{T}}_M \bar{\mathbf{T}}_N}^\Gamma(\mathbf{K}_n) = \frac{1}{N_c} \sum_{R_l R_j} e^{-i\mathbf{K}_n(\mathcal{R}_{lM} - \mathcal{R}_{jN})} F_{\bar{\mathbf{T}}_M \bar{\mathbf{T}}_N}^{\theta, \mathcal{R}_{lM}, \mathcal{R}_{jN}}. \quad (33)$$

It can be found that ADCA self-energy contains the contribution of the crossing diagrams that are absent in ACPA, as illustrated in Fig. 4.

For instance, the first crossing diagram is given by the term $\overline{V^\theta \bar{g}^\theta V^\theta \bar{g}^\theta V^\theta \bar{g}^\theta V^\theta}$, as derived in the following:

$$\begin{aligned} \overline{[V^\Gamma \bar{g}^\Gamma V^\Gamma \bar{g}^\Gamma V^\Gamma \bar{g}^\Gamma V^\Gamma]}(K) &= \frac{1}{N_c} \sum_{I,J} e^{-iK(\mathbf{R}_I - \mathbf{R}_J)} \overline{[V^\theta \bar{g}^\theta V^\theta \bar{g}^\theta V^\theta \bar{g}^\theta V^\theta]_{\mathbf{R}_I \mathbf{R}_J}} \\ &= \frac{1}{N_c} \sum_{I,J,P,L} e^{-iK(\mathbf{R}_I - \mathbf{R}_J)} \overline{[V^{\theta, \mathbf{R}_I} \bar{g}^{\theta, \mathbf{R}_I \mathbf{R}_P} V^{\theta, \mathbf{R}_P} \bar{g}^{\theta, \mathbf{R}_P \mathbf{R}_L} V^{\theta, \mathbf{R}_L} \bar{g}^{\theta, \mathbf{R}_L \mathbf{R}_J} V^{\theta, \mathbf{R}_J}]} \\ &= \frac{1}{N_c^4} \sum_{I,J,P,L} \sum_{\mathbf{K}_1, \mathbf{K}_2, \mathbf{K}_3} e^{-i\mathbf{K}(\mathbf{R}_I - \mathbf{R}_J)} e^{i\mathbf{K}_1(\mathbf{R}_I - \mathbf{R}_P)} e^{i\mathbf{K}_2(\mathbf{R}_P - \mathbf{R}_L)} e^{i\mathbf{K}_3(\mathbf{R}_L - \mathbf{R}_J)} \\ &\quad \times \overline{V^\Gamma \bar{g}^\Gamma(\mathbf{K}_1) V^\Gamma \bar{g}^\Gamma(\mathbf{K}_2) V^\Gamma \bar{g}^\Gamma(\mathbf{K}_3) V^\Gamma}. \end{aligned} \quad (34)$$

For the case of $I = L, P = J, I \neq J$, we can get the first crossing diagram term,

$$\begin{aligned} &\frac{1}{N_c^4} \sum_I \sum_{J(I \neq J)} \sum_{\mathbf{K}_1, \mathbf{K}_2, \mathbf{K}_3} \overline{V^\Gamma \bar{g}^\Gamma(\mathbf{K}_1) V^\Gamma \bar{g}^\Gamma(\mathbf{K}_2) V^\Gamma \bar{g}^\Gamma(\mathbf{K}_3) V^\Gamma} e^{i\mathbf{R}_I(\mathbf{K} + \mathbf{K}_2 - \mathbf{K}_3 - \mathbf{K}_1)} e^{i\mathbf{R}_J(\mathbf{K}_3 + \mathbf{K}_1 - \mathbf{K}_2 - \mathbf{K})} \\ &= \frac{1}{N_c^3} \sum_J \sum_{\mathbf{K}_1, \mathbf{K}_2, \mathbf{K}_3} \overline{V^\Gamma \bar{g}^\Gamma(\mathbf{K}_1) V^\Gamma \bar{g}^\Gamma(\mathbf{K}_2) V^\Gamma \bar{g}^\Gamma(\mathbf{K}_3) V^\Gamma} \delta_{\mathbf{K} + \mathbf{K}_2, \mathbf{K}_3 + \mathbf{K}_1} e^{i\mathbf{R}_J(\mathbf{K}_3 + \mathbf{K}_1 - \mathbf{K}_2 - \mathbf{K})} \\ &\quad - \frac{1}{N_c^3} \sum_{\mathbf{K}_1, \mathbf{K}_2, \mathbf{K}_3} \overline{V^\Gamma \bar{g}^\Gamma(\mathbf{K}_1) V^\Gamma \bar{g}^\Gamma(\mathbf{K}_2) V^\Gamma \bar{g}^\Gamma(\mathbf{K}_3) V^\Gamma} \\ &= \frac{1}{N_c^3} \sum_{\mathbf{K}_1, \mathbf{K}_2, \mathbf{K}_3} \overline{V^\Gamma \bar{g}^\Gamma(\mathbf{K}_1) V^\Gamma \bar{g}^\Gamma(\mathbf{K}_2) V^\Gamma \bar{g}^\Gamma(\mathbf{K}_3) V^\Gamma} N_c \delta_{\mathbf{K} + \mathbf{K}_2, \mathbf{K}_3 + \mathbf{K}_1} \\ &\quad - \frac{1}{N_c^3} \sum_{\mathbf{K}_1, \mathbf{K}_2, \mathbf{K}_3} \overline{V^\Gamma \bar{g}^\Gamma(\mathbf{K}_1) V^\Gamma \bar{g}^\Gamma(\mathbf{K}_2) V^\Gamma \bar{g}^\Gamma(\mathbf{K}_3) V^\Gamma}. \end{aligned} \quad (35)$$

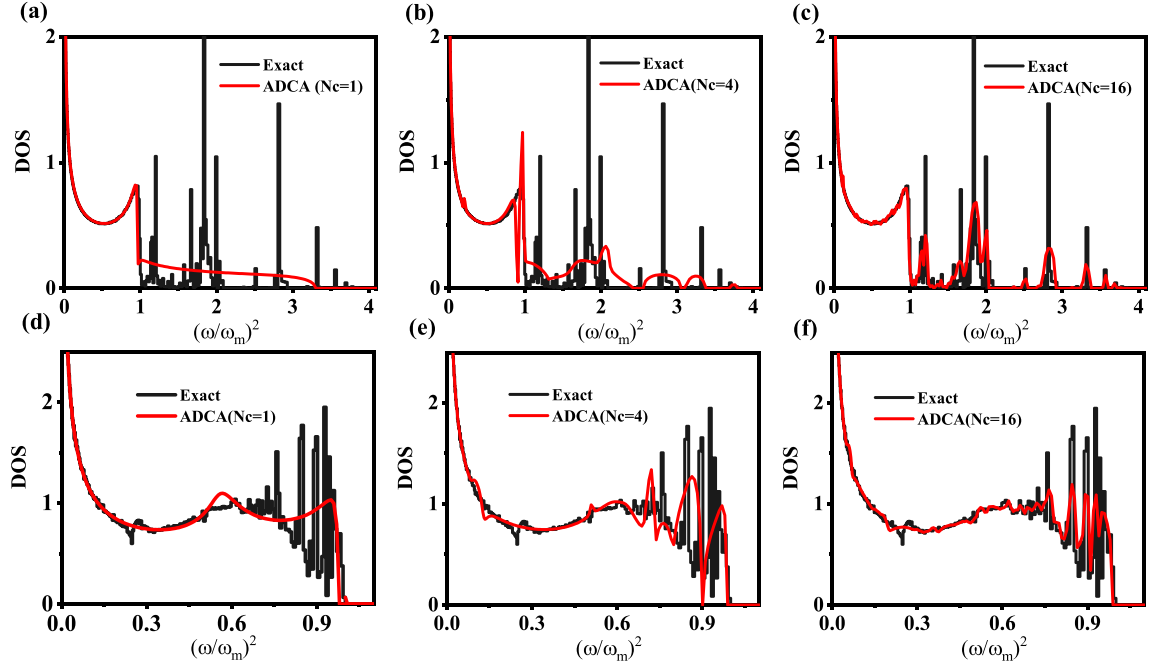


FIG. 5. The averaged density of states of the ADCA with a different cluster size ($N_c = 1, 4, 16$) compared with the exact results (calculated by Dean's technique [48]). Parts (a)–(c) show the system parameters $m_A = 1.0$, $k_{AA} = 1.0$, $m_B = 0.5$, $C_B = 0.3$, $k_{AB} = 1.41$, $K_{BB} = 2.0$, and (d)–(f) are for the system by changing $k_{BB} = 0.25$, $k_{AB} = 0.5$, with other parameters the same as in the first case.

The first term in Eq. (35) includes convolutions of $\bar{g}^\Gamma(\mathbf{K})$, which reflect nonlocal correlation effects. To account for these effects, the ADCA method replaces the lattice propagators $\bar{g}(\mathbf{K} + \tilde{\mathbf{k}})$ with the coarse-grained propagators $\bar{g}^\Gamma(\mathbf{K})$. These coarse-grained propagators are obtained through the ADCA coarse-graining procedure, namely

$$\bar{g}_{\bar{\mathbf{T}}_i \bar{\mathbf{T}}_j}^\Gamma(\mathbf{K}) = \frac{N_c}{N} \sum_{\tilde{\mathbf{k}}} \bar{g}^S(\mathbf{K}, \tilde{\mathbf{k}}) e^{i\tilde{\mathbf{k}}(\bar{\mathbf{T}}_i - \bar{\mathbf{T}}_j)}. \quad (36)$$

VI. NUMERICAL RESULTS AND DISCUSSION

We have implemented the ADCA algorithm and tested the code with $N_c = 1$ to reproduce ACPA results and the case of mass-only disorder (by keeping \mathcal{K}^{R_l} constant for different atomic occupations) to obtain the DCA results. In the following, we present the ADCA mean-field results for both the mass and force-constant disorders in lattice vibration, and we validate the ADCA approach by comparing with the exact results and supercell simulations for the disordered 1D atomic chain and 3D lattice systems.

A. DOS in disordered 1D binary alloys

We first validate ADCA by calculating the disordered 1D atomic chain. The 1D chain features the minimal number of neighboring couplings compared to 2D and 3D systems, and thus presents an important challenge for mean-field approaches in local approximations due to the large fluctuations (especially for ACPA in a single-site approximation, as known from the central limit theorem) [41]. This makes the disordered 1D chain an important testing system for assessing the accuracy and applicability of the ADCA for simulating

off-diagonal disorder. With ADCA, we calculate the arithmetically averaged local density of states (DOS) as follows:

$$\rho(\omega^2) = -\frac{1}{\pi} \frac{1}{N_c} \sum_{\mathbf{R}_l, \mathcal{Q}} c^{\mathcal{Q}} m^{\mathcal{Q}} g_{\bar{\mathbf{T}}_0 \bar{\mathbf{T}}_0}^{\Theta, \mathcal{Q}, \mathbf{R}_l, \mathbf{R}_l} x^{\mathcal{Q}, -1}. \quad (37)$$

Figure 5 presents the ADCA DOS results and the exact results obtained via Dean's technique (by using a 10 000-atom random chain) [48]. Figures 5(a)–5(c) show the results for the system with parameters $m_A = 1.0$, $k_{AA} = 1.0$, $k_{BB} = 2.0$, $k_{AB} = 1.41$, $m_B = 0.5$, $C_B = 0.3$. For simplicity, the frequency is normalized by ω^2/ω_m^2 ($\omega_m = 2\sqrt{\frac{K_{AA}}{m_A}}$). As shown in Fig. 5(a), the defect band in the exact result, separated from the host band $\frac{\omega^2}{\omega_m^2} \leq 1$, exhibits a set of spiky peaks in the high frequency $1 \leq \frac{\omega^2}{\omega_m^2} \leq 4$, due to the highly localized vibrational modes for some specific local structures. It is clear that, at the low frequencies, namely $0 \leq \frac{\omega^2}{\omega_m^2} \leq 1$, the result of $N_c = 1$ agrees very well with the exact DOS, since vibrational modes with long wavelengths are less influenced by disorder. However, for $N_c = 1$, ADCA (namely ACPA) fully fails to accommodate any specific local atomic configuration which requires a cluster, and produces rather smooth DOS results, contrasting the peaks in the exact result. Upon increasing the cluster size to $N_c = 4$, as compared to the result of $N_c = 1$, a great change in DOS can be found at high frequencies in the range of $1 \leq \frac{\omega^2}{\omega_m^2} \leq 4$, while the DOS result for low frequency remains almost unchanged. As shown, some peak structures in the DOS of $N_c = 4$ begin to emerge at high frequencies, illustrating the important influence of some specific alloy structures. However, due to limitations of a small cluster size, the ADCA result of $N_c = 4$ still presents a large deviation

from the exact result, including the omission of some localized modes. Upon further increasing N_c to 16, it is evident that the ADCA DOS produces the exact results very well. Especially in $1 \leq \frac{\omega^2}{\omega_m^2} \leq 4$ by $N_c = 16$ ADCA calculations, each of those peaks due to a localized mode is accurately produced and exhibits a remarkable agreement with the exact DOS results, despite the fact that the peaks are broadened due to the mean-field nature of the approach. It is thus illustrated that, upon further increasing the cluster to the large limit, ADCA can reproduce the exact results. As a mean-field approach with an embedded finite-size cluster, ADCA only accounts for the effects of fluctuations in the local degree of freedom within the cluster, presenting the major difference between ADCA results and exact results in Fig. 5. By increasing the cluster size, ADCA provides a systematic way to improve the accuracy by effectively including the nonlocal correlation of disorder scattering and capturing the effects of specific local alloy configurations. It should be mentioned that MACPA is also capable of producing localized modes for systems with off-diagonal disorder as shown in Fig. 5 [41]. However, an intrinsic issue with MACPA is the violation of the full translational symmetry of the lattice, which is directly addressed by ADCA.

Figures 5(d)–5(f) present the DOS results by changing the system parameters $k_{BB} = 0.25$, $k_{AB} = 0.5$. In this system, the defect band intermingles with the host band. As shown in the exact result of Fig. 5(d), within the defect band, a unique structure characterized by four distinct peaks begins to take shape in the range $0.7 \leq \frac{\omega}{\omega_m} \leq 1.0$. Similar to the peak in the previous case, these peaks are given by the localized modes of some specific local configuration. Increasing a cluster size from $N_c = 1$ to $N_c = 16$ once again provides a substantial improvement of the results to agree with the exact results. Upon examining the $N_c = 16$ results, each of the major peaks can be reproduced in good agreement with the exact results. The ADCA method thus provide an effective mean-field approach to account for the cluster effects of general disorders with the remarkable accuracy controlled by the cluster size.

B. DOS for disordered 3D binary alloys

In this section, we present the ADCA averaged DOS for 3D alloys to further demonstrate the implementation of ADCA. Due to the larger number of neighboring sites, it is expected that ADCA will yield fewer errors for the 3D systems with off-diagonal disorders, compared to the 1D chain. We compare the ACDA results with that obtained by the implementation of the periodic supercell (SC) method. We calculate the simple-cubic lattices with disordered mass and force constants. The simple-cubic lattice features the smallest number of neighboring sites in comparison with bcc and fcc lattices, presenting a good testing 3D system for mean-field theories. For the SC results, we use a supercell size of 125 atoms. and the DOS results are averaged over 1000 random atomic configurations. In the ADCA calculations, we employ 2^8 , 2^{10} , and 2^{10} randomly sampled atomic configurations for the respective cluster size $N_c = 8, 64, 125$. Compared to the disordered 1D lattice, the 3D lattice presents less averaged fluctuation in the environment for embedding each atom, and the spiky structures inherent in the exact

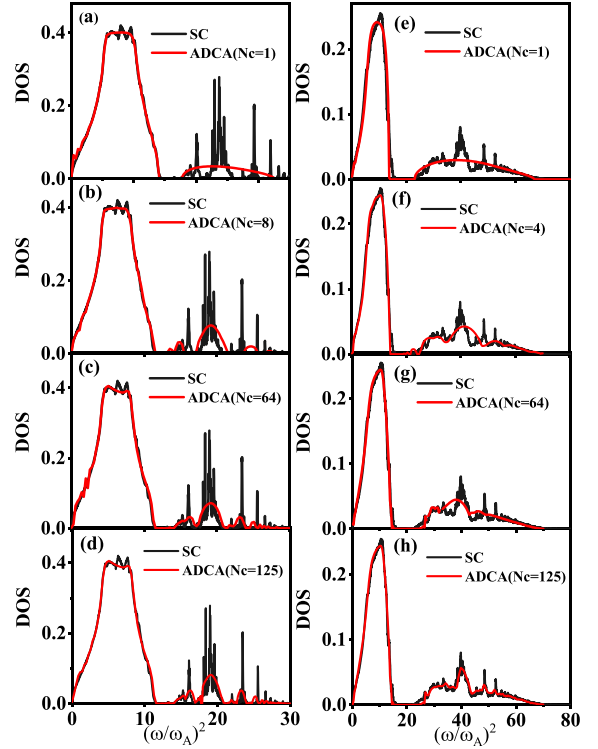


FIG. 6. The phonon density of states for 3D disordered binary alloys with the system parameters (I): (a)–(d) $m_A = 1.0$, $k_{AA} = 1.0$, $m_B = 0.5$, $K_{AB} = 1.414$, $K_{BB} = 2.0$, $C_B = 0.1$, and (II): (e)–(h) $K_{AB} = 3.0$, $K_{BB} = 4.0$, $C_B = 0.3$ with other parameters the same as in the first case. The ADCA results (in red) for different cluster sizes are compared with the supercell calculations (in black).

DOS thus tend to vanish. Consequently, for discussing the validity of the ADCA formalism, we carefully select two sets of system parameters with strong force-constant disorder, including case (I) $m_A = 1.0$, $k_{AA} = 1.0$, $m_B = 0.5$, $K_{AB} = 1.414$, $K_{BB} = 2.0$, $C_B = 0.1$; and case (II) $m_A = 1.0$, $k_{AA} = 1.0$, $m_B = 0.5$, $K_{AB} = 3.0$, $K_{BB} = 4.0$, $C_B = 0.3$ (here we use the same convention for 3D force-constant model as Refs. [20,48] for all 3D lattices in this work). Figure 6 presents the results for case (I) in Figs. 6(a)–6(d) and for case (II) in Figs. 6(e)–6(h) for different ADCA clusters in comparison with SC results. For simplicity, the frequency is normalized by ω^2/ω_A^2 ($\omega_A = \sqrt{\frac{K_{AA}}{m_A}}$).

As shown in the SC results for both cases, the host and defect bands are unequivocally differentiated, and the DOS results for a defect band lying at high frequencies present evident features of localized modes, namely the pronounced peaks, especially in case (I). Within the host band at the low-frequency region ($\frac{\omega^2}{\omega_A^2} \leq 15$), the ADCA results, even with $N_c = 1$, agree very well with the SC calculations, presenting an important test for the correct implementation of ADCA for 3D lattices. Similar to the 1D lattice, increasing the cluster size almost does not change the results in the host band in ADCA calculations, due to the weak scattering for which the single-site approximation ($N_c = 1$) already can provide very satisfactory results. For the defect bands ($\frac{\omega^2}{\omega_A^2} \geq 15$) of

both cases, ADCA with $N_c = 1$ always produces a smooth and monotonous profile, deviating from the SC results with peaks. However, by increasing the cluster size, ADCA refines the results in the high-frequency region and produces pronounced peaks to approach the results of SC, corroborating the ADCA formalism. Compared to case (II), ADCA for case (I) exhibits a quicker convergence with respect to the cluster size N_c , due to the relatively weaker scattering of disorder as seen from the system parameters. For example, ADCA with $N_c = 64$ reaches a good agreement with the SC calculations for case (I) by reproducing well the four major DOS peaks in $15 \leq \frac{\omega^2}{\omega_A^2} \leq 30$, while case (II) requires ADCA with $N_c = 125$ to produce well the SC results. Here, it should be mentioned that SC and ADCA utilize thoroughly different boundary conditions, presenting distinct simulation efficiency. By applying to the 1D and 3D alloys, we have demonstrated the important effectiveness of the ADCA approach to handle off-diagonal disorder for simulating realistic materials.

C. Geometrically averaged DOS for 3D alloys

In the previous sections, the presented DOS results are obtained by the arithmetic average as shown in Eq. (37). It is known that a complete statistical description of random quantities requires the probability distribution function (PDF). However, in many cases, the PDF is not known, and only limited information about the system, provided by certain moments or cumulants, is available. For example, the first moment is known as the arithmetic average. The arithmetic average, such as the arithmetically averaged density of states (ADOS), cannot give a description of the spatial distribution, which can be strongly dependent on the local configuration of the alloy. For a disordered system with strong fluctuation in the local DOS (LDOS), the ADOS does not resemble its typical value at all, needing further information. For a disordered material, an important effect is the localization given by the interference of disorder scattering, which requires the information of the LDOS distribution to characterize. For example, the LDOS closes to zero at some sites upon approaching the localization. Thus, a quantity is required to detect the localization for a disordered system. As a supplement to the ADOS which averages out the fluctuations, the geometrically averaged DOS (GDOS) can provide important information about the spatial fluctuation of the LDOS. In other literature, the GDOS is also referred to as typical density of states (TDOS) [47]. The difference between ADOS and GDOS provides a simple and straightforward way to describe the fluctuations and the extent of localization.

Different from the typical medium DCA (TMDCA) [34,35], we construct here the GDOS directly using the quantities in ADCA, namely

$$\rho_g(\omega^2) = -\frac{1}{\pi} \exp \left[\frac{1}{N_C} \sum_{\mathbf{R}_l, \mathcal{Q}} \ln(m_{\mathcal{Q}}^{\mathcal{Q}} g_{\mathbf{T}_0 \mathbf{T}_0}^{\mathcal{Q}, \mathcal{Q}} \mathbf{R}_l \mathbf{R}_l x_{\mathcal{Q}, -1}^{\mathcal{Q}}) \right].$$

In Fig. 7, we present a comparison of ADOS and GDOA for 3D lattices with different disordered parameters to investigate how the interplay of mass and force-constant disorders effects the localization of phonon modes [49]. (It should be noted that we are not intending to provide a strict theory to characterize

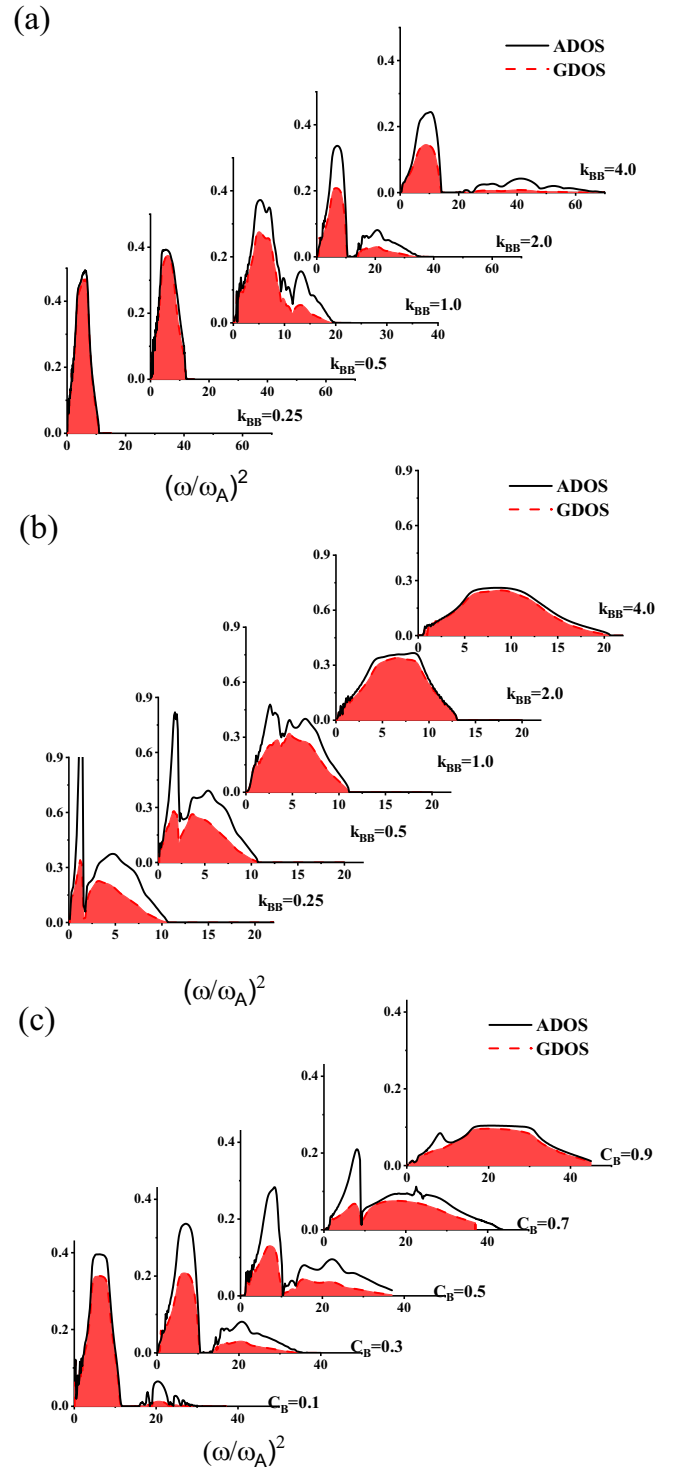


FIG. 7. Comparison of GDOS (red shaded) and ADOS (solid black line) calculated with ADCA ($N_c=64$) for different 3D simple-cubic systems (with the host $m_A = 1.0$, $K_{AA} = 1.0$). Part (a) is for the parameters $m_B = 0.5$, $C_B = 0.3$ with varied K_{BB} ; (b) is for the parameters $m_B = 2.0$, $C_B = 0.3$ with varied K_{BB} ; (c) is for the parameters $m_B = 0.5$, $K_{BB} = 2.0$ with varied C_B from 0.1 to 0.9. For all systems, $K_{AB} = 0.6K_{BB} + 0.4K_{AA}$.

the localization of phonon in this work.) For all the systems, we use the host parameters $m_A = 1$, $k_{AA} = 1.0$.

In Fig. 7(a), we present the results for systems with $m_B = 0.5$, $k_{AB} = 0.6k_{BB} + 0.4k_{AA}$, and $c_B = 0.3$, and different k_{BB} changing from the soft 0.25 to very stiff 4.0. As shown, for the case of $k_{BB} = 0.25$, the defect band lies deep inside the host band, which features the low frequency $\frac{\omega^2}{\omega_A^2} \leq 10$, and it presents a tiny difference in ADOS and GDOS, illustrating the weak disorder scattering. As k_{BB} increases, the difference between ADOS and GDOS is increased and the defect band emerges. For $k_{BB} = 1.0$ corresponding to the mass-only disorder, the bandwidth of the alloy is significantly enlarged, and the second peak, representing the defect band, appears at a relatively high frequency compared to the results of $k_{BB} = 0.25$. Upon further increasing k_{BB} to the value 2.0 and 4.0, the defect band is clearly separated from the host. Meanwhile, for $k_{BB} \geq 1.0$, it is evident that the GDOS is significantly reduced compared to the ADOS in a large range of frequencies, demonstrating the disorder-induced large fluctuation in the LDOS. For $k_{BB} = 4.0$, the GDOS in defect band $\frac{\omega^2}{\omega_A^2} \geq 20$ is almost eliminated, presenting an almost localized vibrational mode. Moreover, GDOS at the low-frequency region of the host band is also significantly decreased compared to ADOS, presenting the important influence of disorder. The examples shown in Fig. 7(a) demonstrate an important interplay of mass and force-constant disorder, namely that the increase of k_{BB} over 1.0 for the case $m_B = 0.5$ can enhance the localization effect in the phonon mode, while decreasing k_{BB} below 1.0 delocalizes the results as compared to the result of mass-only disorder.

To further explore the interplay of mass and force-constant disorders, in Fig. 7(b) we show results for the case $m_B = 2.0$ with other parameters the same as Fig. 7(a). By changing k_{BB} , the results of $m = 2.0$ present the opposite trend compared to the results of $m = 0.5$ as shown in Fig. 7. For example, upon reducing k_{BB} to 0.25, in contrast to the $m = 0.5$ case, the spiky peak for the defect band is presented at very low frequency, and moreover the difference between the ADOS and GDOS is becoming evident even at the very low frequency region, illustrating the important extent of localization at these frequencies. However, on the other hand, increasing k_{BB} will narrow the difference between ADOS and GDOS; for example, at $k_{BB} = 4.0$, GDOS shows a very close result to the ADOS, presenting an important delocalization effect of force-constant disorder. To further investigate the effect of disorders, in Fig. 7(c) we present the ADOS and GDOS with different concentrations of B atom c_B , for the specific case $m_B = 0.5$, $K_{BB} = 2.0$ [with other parameters the same as the cases in Fig. 7(a)]. Upon increasing c_B above 0.5, it is clear that the defect (A atom) and host band merge together, and the difference between ADOS and GDOS can be reduced to present the delocalization tendency in a large range of frequency. As found for the low $c_B = 0.1$, the separated defect (B atom) band at high frequency tends to be localized, while the host (A atom) band at the low-frequency region remains largely extended, as seen from the small difference between ADOS and GDOS. Based on the results for systems with both the diagonal and off-diagonal disorders in Fig. 7, it is clear that the off-diagonal disorder can play very important roles in determining the lattice vibrational properties, presenting both enhanced localization and delocalization effects. Therefore,

including off-diagonal disorder is critical for the simulation of disordered materials, and the development of ADCA provides an effective approach for simulating both diagonal and off-diagonal disorder on the same theoretical footing.

VII. CONCLUSION

As a summary, we have reported a self-consistent auxiliary dynamical cluster theory, namely ADCA, to effectively account for the cluster effects of off-diagonal disorder. We introduced the coupling space to encapsulate the extended local degree of freedom to describe the off-diagonal disorder in the auxiliary medium. In this method, by utilizing the cluster coupling space, the impurity cluster with the enforced BVK periodic boundary condition is homogeneously treated to conserve full symmetry of the lattice. ADCA restores ACPA in the single-site limit, and DCA for the diagonal-only disorder. To demonstrate the correct implementation of ADCA, we have shown that, for disordered lattice vibration, by using an appropriate cluster size, ADCA can produce the density of states of phonons close to the exact results for a 1D chain and supercell results for a 3D lattice, especially for those localized defect modes. As an important application, with ADCA we investigated the important interplay of mass and force-constant disorders by calculating the geometrically and arithmetically averaged density of states, and we found that the force-constant disorder can significantly modulate the localization extent of both the host and defect states, presenting both enhanced localization and delocalization. This work, by developing ADCA, provides an effective approach for simulating profound effects of both diagonal and off-diagonal disorder in materials. In this work, we only considered the disordered phonon system, but the application of ADCA to an electronic system is straightforward, for example to treat the electron transport in disordered nanoelectronics, and to combine with the DMFT to handle a strongly correlated electronic system with atomic disorder.

ACKNOWLEDGMENTS

Y.K. acknowledges financial support from NSFC (Grant No. 12227901). The authors thank the HPC platform of ShanghaiTech University for providing the computational facility.

APPENDIX A: THE MCPA AND DCA HOPPING MATRIX IN COUPLING SPACE

Both the conventional DCA and the MCPA for diagonal disorder address the problem of embedding a cluster within an effective medium. However, the coupling of the cluster to the medium adheres to different boundary conditions for each method, resulting in different expression in reciprocal space.

In MCPA, the cluster-averaged Green's function (in the cluster space \mathcal{C}) can be written as

$$\hat{G}^{\mathcal{C}, \text{MCPA}} = \frac{N_c}{N} \sum_{\vec{k}} G^{\mathcal{C}, \text{MCPA}}(\vec{k}) \quad (\text{A1})$$

$$= \frac{N_c}{N} \sum_{\vec{k}} [\hat{\mathcal{P}}^{\mathcal{C}, \text{MCPA}} + \hat{W}^{\mathcal{C}, \text{MCPA}}(\vec{k})]^{-1}, \quad (\text{A2})$$

where $\hat{\mathcal{P}}^{\text{MCPA}}$ denotes the cluster effective medium and is a cluster-diagonal quantity. Here, $\hat{W}_{\text{MCPA}}(\tilde{\mathbf{k}})$ represents the periodic hopping (coupling) term obtained by normal cluster Fourier transformation. As an example, we consider a 1D chain with a lattice constant a and an ordered nearest-neighbor hopping W , for which we have

$$\hat{W}^{\mathcal{C},\text{MCPA}}(\tilde{\mathbf{k}}) = \begin{pmatrix} \ddots & w & e^{-i\tilde{\mathbf{k}}(N_c a)w} \\ w & & w \\ & w & w \\ e^{-i\tilde{\mathbf{k}}(-N_c a)w} & w & \ddots \end{pmatrix}. \quad (\text{A3})$$

After mapping to the cluster coupling space, we can get the nonzero elements,

$$\hat{W}_{\bar{\mathbf{T}}_0 \bar{\mathbf{T}}_0}^{\ominus, \text{MCPA}} = \begin{pmatrix} \ddots & w & & \\ w & & w & \\ & w & & w \\ & & w & \ddots \end{pmatrix}, \quad (\text{A4})$$

$$\hat{W}^{\mathcal{C},\text{DCA}}(\tilde{\mathbf{k}}) = \begin{pmatrix} \ddots & w e^{-i\tilde{\mathbf{k}}(-1)a} & & e^{-i\tilde{\mathbf{k}}(N_c - N_c + 1)a} w \\ w e^{-i\tilde{\mathbf{k}}(1)a} & & w e^{-i\tilde{\mathbf{k}}(-1)a} & \\ & w e^{-i\tilde{\mathbf{k}}(1)a} & & w e^{-i\tilde{\mathbf{k}}(-1)a} \\ e^{-i\tilde{\mathbf{k}}(-N_c + N_c - 1)a} w & & w e^{-i\tilde{\mathbf{k}}(1)a} & \ddots \end{pmatrix} \quad (\text{A9})$$

in which all sites are homogeneously handled, different from the MCPA. However, to uphold translational symmetry in DCA, the concept of real space is forfeited. Therefore, we can map to the cluster coupling space to obtain

$$\hat{W}_{\bar{\mathbf{T}}_0 \bar{\mathbf{T}}_0}^{\text{DCA}} = \begin{pmatrix} \ddots & 0 & & \\ 0 & & 0 & \\ & 0 & & 0 \\ & & 0 & \ddots \end{pmatrix}, \quad (\text{A10})$$

$$\hat{W}_{\bar{\mathbf{T}}_0 \bar{\mathbf{T}}_{+1}}^{\text{DCA}} = \begin{pmatrix} \ddots & w & & \\ & & w & \\ w & & & w \\ & w & & \ddots \end{pmatrix}, \quad (\text{A11})$$

$$\hat{W}_{\bar{\mathbf{T}}_0 \bar{\mathbf{T}}_{-1}}^{\text{DCA}} = \begin{pmatrix} \ddots & & & w \\ w & & & \\ & w & & \\ & & w & \ddots \end{pmatrix}, \quad (\text{A12})$$

where $\bar{\mathbf{T}}_{-1} = -a$ and $\bar{\mathbf{T}}_{+1} = a$.

and two coupling term between the cluster,

$$\hat{W}_{\bar{\mathbf{T}}_0 \bar{\mathbf{T}}_{+1}}^{\ominus, \text{MCPA}} = \begin{pmatrix} \ddots & & & \\ & w & & \ddots \\ & & & \\ & & & w \end{pmatrix}, \quad (\text{A5})$$

$$\hat{W}_{\bar{\mathbf{T}}_0 \bar{\mathbf{T}}_{-1}}^{\ominus, \text{MCPA}} = \begin{pmatrix} \ddots & & & \\ & & & w \\ & & & \\ & & & \ddots \end{pmatrix}, \quad (\text{A6})$$

where $\bar{\mathbf{T}}_{-1} = -aN_c$, and $\bar{\mathbf{T}}_{+1} = aN_c$ for the coupling space of a cluster. It is clear that in MCPA, the cluster sites cannot be equivalently treated, thus presenting a cluster approach with an open boundary condition.

For DCA in which the BVK periodic boundary is enforced in the cluster, the averaged Green's function in cluster space \mathcal{C} is given by

$$\hat{G}^{\mathcal{C},\text{DCA}} = \frac{N_c}{N} \sum_{\tilde{\mathbf{k}}} G^{\mathcal{C},\text{DCA}}(\tilde{\mathbf{k}}) \quad (\text{A7})$$

$$= \frac{N_c}{N} \sum_{\tilde{\mathbf{k}}} [\hat{\mathcal{P}}^{\mathcal{C},\text{DCA}}(\tilde{\mathbf{k}}) + \hat{W}^{\mathcal{C},\text{DCA}}(\tilde{\mathbf{k}})]^{-1}. \quad (\text{A8})$$

However, by maintaining translational symmetry, the DCA's hopping (coupling) term is known as, for a 1D chain,

APPENDIX B: ADCA FOR MASS-ONLY (DIAGONAL) DISORDER

In this Appendix, we will see that the ADCA condition equals the DCA condition when considering the mass-only disorder, for which we keep \mathcal{K}^{R_l} the same for all sites in the cluster. To do so, we first rewrite the quantity $g^{\ominus, Q-1} = P^{\ominus, Q} - \Omega^{\ominus}$ as a block centrosymmetric matrix (guaranteed by the properties of auxiliary physical quantities) as

$$g^{\ominus, Q-1} = \begin{pmatrix} A & M & B \\ N & Q & N \\ B & M & A \end{pmatrix}, \quad (\text{B1})$$

where only the Q matrix containing the mass is configuration-dependent, which corresponds to the $g_{\bar{\mathbf{T}}_0 \bar{\mathbf{T}}_0}^{\ominus, Q-1}$ in coupling space.

We can first rewrite $g^{\ominus, Q-1}$ as

$$U g^{\ominus, Q-1} U^T = \begin{pmatrix} A - B & 0 & 0 \\ 0 & Q & \sqrt{2}N \\ 0 & \sqrt{2}M & A + B \end{pmatrix}, \quad (\text{B2})$$

where U is

$$U = \begin{pmatrix} I/\sqrt{2} & 0 & -I/\sqrt{2} \\ 0 & I & 0 \\ I/\sqrt{2} & 0 & I/\sqrt{2} \end{pmatrix}. \quad (\text{B3})$$

Then, we can diagonalize $g^{\Theta, Q-1}$ by

$$F^N U g^{\Theta, Q-1} U^T F^M = \begin{pmatrix} A-B & 0 & 0 \\ 0 & \alpha^Q & 0 \\ 0 & 0 & A+B \end{pmatrix}, \quad (\text{B4})$$

where $\alpha^Q = Q - 2N(A+B)^{-1}M$, and

$$F^N = \begin{pmatrix} I & 0 & 0 \\ 0 & I & -\sqrt{2}N(A+B)^{-1} \\ 0 & 0 & I \end{pmatrix}, \quad (\text{B5})$$

$$F^M = \begin{pmatrix} I & 0 & 0 \\ 0 & I & 0 \\ 0 & -\sqrt{2}M(A+B)^{-1} & I \end{pmatrix}. \quad (\text{B6})$$

Thus the ADCA condition can be written as

$$\begin{aligned} \sum_Q c^Q g^{\Theta, Q} &= U F^N \begin{pmatrix} (A-B)^{-1} & 0 & 0 \\ 0 & \sum_Q c^Q \alpha^{Q-1} & 0 \\ 0 & 0 & (A+B)^{-1} \end{pmatrix} F^M U^T = U F^N \begin{pmatrix} (A-B)^{-1} & 0 & 0 \\ 0 & \alpha_{\text{mass}}^{-1} & 0 \\ 0 & 0 & (A+B)^{-1} \end{pmatrix} F^M U^T \\ &= \begin{pmatrix} A & M & B \\ N & P_{\text{mass}} & N \\ B & M & A \end{pmatrix}^{-1} = (\mathcal{P}^{\Theta} - \Omega^{\Theta})^{-1}, \end{aligned} \quad (\text{B7})$$

where $P_{\text{mass}} = \alpha_{\text{mass}} + 2N(A+B)^{-1}M$. Then we obtain the DCA condition

$$\sum_Q c^Q (P_{\bar{T}_0 \bar{T}_0}^{\Theta, Q} - \Omega_{\text{DCA}})^{-1} = (P_{\bar{T}_0 \bar{T}_0}^{\Theta} - \Omega_{\text{DCA}})^{-1}, \quad (\text{B8})$$

where $\Omega_{\text{DCA}} = \Omega_{\bar{T}_0 \bar{T}_0}^{\Theta} - 2N(A+B)^{-1}M$, for which the last term $2N(A+B)^{-1}M$ remains constant in the self-consistent mean-field calculations.

- [1] S. de Gironcoli and S. Baroni, *Phys. Rev. Lett.* **69**, 1959 (1992).
 [2] Y. F. Ye, Q. Wang, J. Lu, C. T. Liu, and Y. Yang, *Mater. Today* **19**, 349 (2016).
 [3] D. B. Miracle and O. N. Senkov, *Acta Mater.* **122**, 448 (2017).
 [4] E. P. George, D. Raabe, and R. O. Ritchie, *Nat. Rev. Mater.* **4**, 515 (2019).
 [5] E. Ma and X. L. Wu, *Nat. Commun.* **10**, 5623 (2019).
 [6] E. P. George, W. A. Curtin, and C. C. Tasan, *Acta Mater.* **188**, 435 (2020).
 [7] Z. Li, K. G. Pradeep, Y. Deng, D. Raabe, and C. C. Tasan, *Nature (London)* **534**, 227 (2016).
 [8] T. Yang, Y. L. Zhao, Y. Tong, Z. B. Jiao, J. Wei, J. X. Cai, X. D. Han, D. Chen, A. Hu, J. J. Kai, K. Lu, Y. Liu, and C. T. Liu, *Science* **362**, 933 (2018).
 [9] Z. F. Lei, X. J. Liu, Y. Wu, H. Wang, S. H. Jiang, S. D. Wang, X. D. Hui, Y. D. Wu, B. Gault, P. Kontis, D. Raabe, L. Gu, Q. H. Zhang, H. W. Chen, H. T. Wang, J. B. Liu, K. An, Q. S. Zeng, T.-G. Nieh, and Z. P. Lu, *Nature (London)* **563**, 546 (2018).
 [10] B. Gludovatz, A. Hohenwarter, K. V. S. Thurston, H. Bei, Z. Wu, E. P. George, and R. O. Ritchie, *Nat. Commun.* **7**, 10602 (2016).
 [11] C. Liu, *Metall. Trans.* **4**, 1743 (1973).
 [12] P. Singh, A. V. Smirnov, and D. D. Johnson, *Phys. Rev. B* **91**, 224204 (2015).
 [13] A. Fernández-Caballero, J. S. Wrbel, P. M. Mummery, and D. Nguyen-Manh, *J. Phase Eq. Diff.* **38**, 391 (2017).
 [14] Y. Zou, H. Ma, and R. Spolenak, *Nat. Commun.* **6**, 7748 (2015).
 [15] P. Koželj, S. Vrtnik, A. Jelen, S. Jazbec, Z. Jaglicic, S. Maiti, M. Feuerbacher, W. Steurer, and J. Dolinsek, *Phys. Rev. Lett.* **113**, 107001 (2014).
 [16] B. Gludovatz, A. Hohenwarter, D. Catoor, E. H. Chang, E. P. George, and R. O. Ritchie, *Science* **345**, 1153 (2014).
 [17] P. Soven, *Phys. Rev.* **156**, 809 (1967).
 [18] D. W. Taylor, *Phys. Rev.* **156**, 1017 (1967).
 [19] P. Leath, *Phys. Rev.* **171**, 725 (1968).
 [20] R. J. Elliott, J. A. Krumhansl, and P. L. Leath, *Rev. Mod. Phys.* **46**, 465 (1974).
 [21] B. Velicky, S. Kirkpatrick, and H. Ehrenreich, *Phys. Rev.* **175**, 747 (1968).
 [22] P. Soven, *Phys. Rev. B* **2**, 4715 (1970).
 [23] H. Shiba, *Prog. Theor. Phys.* **46**, 77 (1971).
 [24] I. A. Abrikosov and H. L. Skriver, *Phys. Rev. B* **47**, 16532 (1993).
 [25] F. Ducastelle, *J. Phys. C* **4**, L75 (1971).
 [26] F. Ducastelle, *J. Phys. C* **7**, 1795 (1974).
 [27] B. G. Nickel and W. H. Butler, *Phys. Rev. Lett.* **30**, 373 (1973).
 [28] R. Mills, L. J. Gray, and T. Kaplan, *Phys. Rev. B* **27**, 3252 (1983).
 [29] M. Tsukada, *J. Phys. Soc. Jpn.* **32**, 1475 (1972).

- [30] M. H. Hettler, A. N. Tahvildar-Zadeh, M. Jarrell, T. Pruschke, and H. R. Krishnamurthy, *Phys. Rev. B* **58**, R7475 (1998).
- [31] M. H. Hettler, M. Mukherjee, M. Jarrell, and H. R. Krishnamurthy, *Phys. Rev. B* **61**, 12739 (2000).
- [32] M. Jarrell and H. R. Krishnamurthy, *Phys. Rev. B* **63**, 125102 (2001).
- [33] T. Maier, M. Jarrell, T. Prushke, and M. H. Hettler, *Rev. Mod. Phys.* **77**, 1027 (2005).
- [34] C. E. Ekuma, H. Terletska, K. M. Tam, Z. Y. Meng, J. Moreno, and M. Jarrell, *Phys. Rev. B* **89**, 081107(R) (2014).
- [35] H. Terletska, C. E. Ekuma, C. Moore, K. M. Tam, J. Moreno, and M. Jarrell, *Phys. Rev. B* **90**, 094208 (2014).
- [36] J. A. Blackman, D. M. Esterling, and N. F. Berk, *Phys. Rev. B* **4**, 2412 (1971).
- [37] W. R. Mondal, T. Berlijn, M. Jarrell, and N. S. Vidhyadhiraja, *Phys. Rev. B* **99**, 134203 (2019).
- [38] S. Ghosh, P. L. Leath, and M. H. Cohen, *Phys. Rev. B* **66**, 214206 (2002).
- [39] A. Mookerjee, *J. Phys. C* **6**, 1340 (1973).
- [40] J. Zhai, R. Xue, Z. Cheng, and Y. Ke, *Phys. Rev. B* **104**, 024205 (2021).
- [41] Z. Cheng, J. Zhai, Q. Zhang, and Y. Ke, *Phys. Rev. B* **99**, 134202 (2019).
- [42] Z. Cheng, M. Sang, J. Zhai, and Y. Ke, *Phys. Rev. B* **100**, 214206 (2019).
- [43] Q. Wei, J. Zhai, Z. Ning, and Y. Ke, *Phys. Rev. B* **106**, 214205 (2022).
- [44] Z. Zhang, J. Yan, and Y. Ke (unpublished).
- [45] Y. Zhang, Q. Zhang, Y. Ke, and K. Xia, *Chin. Phys. Lett.* **39**, 087301 (2022).
- [46] Y. Zhang, J. Zhai, Z. Chen, Q. Zhang, and Y. Ke, *Phys. Rev. B* **104**, 115412 (2021).
- [47] V. Dobrosavljevic, A. A. Pastor, and B. K. Nikolic, *Europhys. Lett.* **62**, 76 (2003).
- [48] P. Dean, *Rev. Mod. Phys.* **44**, 127 (1972).
- [49] J. Zhai, Q. Zhang, Z. Cheng, J. Ren, Y. Ke, and B. Li, *Phys. Rev. B* **99**, 195429 (2019).